Publ. Astron. Soc. Aust., 2000, 17, 92–101

Catalogue of $J = 1$–0 CO Emission towards Southern Dark Clouds

R. E. Otrupcek[1],* M. Hartley[2] and J.-S. Wang[3]

[1]Mopra Radio Observatory, ATNF, CSIRO, PO Box 309, Coonabarabran, NSW 2357, Australia
rotrupce@atnf.csiro.au
[2] UK Schmidt Telescope, Siding Spring Observatory, Coonabarabran, NSW 2357, Australia
[3] Purple Mountain Observatory, Academia Sinica, Nanjing, China

Received 1999 November 23, accepted 2000 January 19

Abstract: Using the 22-m 'Mopra' antenna (near Coonabarabran, NSW) of the Australia Telescope National Facility (ATNF), we have observed emission from the 115-GHz $J = 1$–0 transition of CO towards the centre of each of the 1101 clouds listed in the Catalogue of Southern Dark Clouds (SDC) of Hartley et al. (1986). The velocity range covered was -96 to $+70$ km s^{-1}, with a velocity resolution of $0{\cdot}120$ km s^{-1}. CO was detected at 1049 of the positions, with 367 spectra showing emission at more than one radial velocity. Here we present the most comprehensive general survey of the SDC catalogue, with the intensity, velocity and half-width of the CO detection and a code describing the profile shape. The presence of blue- or red-shifted wings in many observations can provide a starting point in searches for star-forming regions.

Keywords: catalogues—ISM: clouds—ISM: molecules

1 Introduction

Carbon monoxide is an effective tracer of molecular clouds. Its line emission at microwave frequencies occurs at relatively low excitation and its abundance is second only to molecular hydrogen. It is routinely used to probe the structure of individual clouds in our Galaxy (van Dishoeck & Black 1987). Mapping across dark clouds may reveal changes in the line profiles, which is often due to the clumpy structure of molecular clouds (Blitz 1991). High- and low-velocity line wings of CO emission are well-known signatures of outflowing gas and can indicate the very early stage of stellar evolution (Lada 1985).

Since the 4-m, mm-wave radio telescope at ATNF Headquarters was decommissioned in 1987 there has been no Australian facility for radio observations in the 86–116 GHz frequency range, and therefore no opportunity in Australia for systematic CO observations of dark clouds in the far south. However, the Australia Telescope's 22-m antenna at Mopra is now outfitted for high-frequency operation, and this telescope has been used to complete a set of observations of the $J = 1$–0 transition of CO ($115{\cdot}271$ GHz) in dark clouds further south than declination $-33°$. Some of the dark cloud positions in the catalogue of Hartley et al. (1986) have been observed at lower frequencies, such as 4830 MHz (formaldehyde) and in the Goss et al. (1980) formaldehyde survey there were 169 detections obtained from the 226 positions targetted, providing a useful probe of the properties of those clouds.

2 Observations

The observations were made in 1995 October with the Mopra radio telescope. At that time, the inner 15 m of the reflecting surface had solid panels, enabling the telescope to be effectively used at wavelengths down to $2{\cdot}6$ mm. At 115 GHz the full width at half maximum (FWHM), or beamwidth, is 43 arcsec. The observations were obtained with a dual-channel, cryogenically cooled SIS receiving system. One channel was tuned to the SiO $J = 2$–1, $v = 1$ transition at $86{\cdot}243$ GHz for regular pointing checks at SiO maser positions; the pointing accuracy was found to be better than 10 arcsec. The other channel was tuned to the rest frequency of the CO $J = 1$–0 transition ($115{\cdot}271204$ GHz). The single-sideband receiver temperature was 150 K. The spectra were obtained using a correlator system similar to, but smaller than, that described by Wilson et al. (1992). A bandwidth of 64 MHz over 1024 correlator channels provided a velocity range of 166 km s^{-1} and a velocity resolution of $0{\cdot}195$ km s^{-1}. The velocity 0 km s^{-1} was placed at

* Permission to access the data files containing the observed profiles can be obtained by contacting the principal author.

 10.1071/AS00013 1323-3580/00/010092$05.00

channel 592 to cover as much of the range −150 to +50 km s^{-1} observed in the CO longitude survey (Robinson et al. 1988), which indicated that most of the emission will be in that range.

The target positions were the 1101 entries of the Catalogue of Southern Dark Clouds (hereafter SDC; Hartley et al. 1986) and we observed CO emission along the line of sight of these visual dark clouds. We chose 11 reference positions free from emission 5° off the Galactic Plane and observed one of these for every 10 target positions. The integration time for each observation was 4 min yielding an rms noise of 0·48 K [T_A^* (SEST)]. All observations in our final list were made with an elevation angle >40°. We made several 'sky-dip' observations each day noting the change in gated total power with elevation, so that we could calculate the atmospheric attenuation as a function of the antenna's elevation angle. Several times each day we also observed the bright CO emission at the SiO maser position in Orion [RA (1950): 05 32 47, Dec (1950): −05 24 22] and towards M17 [RA (1950): 18 17 30, Dec (1950): −16 12 59] to establish the antenna gain as a function of elevation, and thus establish an elevation dependent antenna temperature calibration.

The on-line spectral program provided a quotient of CO spectrum and reference spectrum. During off-line processing a linear baseline was removed. The spectral intensities were transformed into a scale of corrected antenna temperature above the atmosphere (T_A^*) in the following way.

The sky-dip observations were used in the temperature relation

$$T_A = T_{obs}\ e\ \tau\ \sec\ Z\,,$$

where T_{obs} is the observed intensity, τ the zenith opacity of the sky, and Z the zenith angle of the telescope. The τ obtained from the sky-dips had a median value of 0·27. The values varied within ±0·03 over the 14-day period, the same as the 'variance' during each day. This constancy reflected continuous dry, clear weather. This value was applied to the peak intensities of the Orion observations (with elevation >40°) but the results still sat on an exponential curve. A solution for τ was calculated that produced constant peak intensity for Orion independent of zenith angle. The use of the new value of 0·51 for τ resulted in an average peak antenna temperature (above the atmosphere) of 11·8 K (±1·4 K) for the Orion CO emission. A scaling value of 6·02 was necessary to bring Orion intensities up to 71 K, the corrected antenna temperature T_A^* observed with the Swedish ESO sub-millimetre telescope (SEST) (L.-A. Nyman, personal communication 1996). (Note that the SEST calibrator list is available on the World Wide Web at www.ls.eso.org/lasilla.Telescope/SEST/SEST html.) The following temperature calibration was then applied to the 1101 observations:

$$T_A^*(\mathrm{SEST}) = 6{\cdot}02\,T_{obs}\,e\,0{\cdot}51\sec Z$$

(henceforth referred to as T_A^*). To calibrate velocity, no Doppler tracking of frequency was done, and the passband of the observing channel was set so that the rest frequency of CO occurred in channel 592. Using an off-line program, observed CO velocities were corrected to local standard of rest for the epoch of observation. Because of a truncation of centre frequency in the menu of the spectral observing program, an error in velocity increased with distance away from channel 592. This error has not been corrected resulting in an error in the velocity that varies between 1·6 km s^{-1} at −90 and 0·9 at +40 km s^{-1}.

3 Results

A total of 1623 independent features were identified in the CO spectra. Gaussian curves were fitted to these features to provide the peak corrected antenna temperature T_A^*, the LSR radial velocity V(LSR) of the centre of the Gaussian curve in km s^{-1}, and a half-power velocity width (FWHM) in km s^{-1}. The median deviation of the Gaussian fits was 0·53 K. The results of the analysis are listed in Table 1. Only the first page of Table 1 is reproduced here. The complete Table 1 is available in postscript format electronically from the Electronic PASA site at

http://www.atnf.csiro.au/pasa/171/otrupcek/table1.html.

The first five columns of Table 1 contain identifying information from Hartley et al. (1986). Column 1 lists the cloud designation in Galactic coordinates; column 2 is RA (B1950); column 3 is Dec (B1950); column 4 is the optical density code (A, B, C); and column 5 lists angular dimensions.

The opacity class in column 4 has retained the label 'Density' to comply with the published Catalogue (Hartley et al. 1986). The results of the Gaussian curve fitting are T_A^*, V (LSR), and FWHM listed in columns 6–8. We felt that the observations were insufficiently described by the parameters of the fitted Gaussians and, as most of the profile shapes tended to fall into groups, a code for the profile shape (a–e) has been added in column 9.

The following is a list of categories used as the code in column 9 of Table 1 that describe the shape of the observed profiles. Lower-case letters were chosen to avoid confusion with the optical density codes from the Hartley et al. catalogue:

a: well-defined narrow Gaussian-shaped spectra with FWHM usually <1·0 km s^{-1}, an rms of fitted Gaussian <0·5 K and, mostly, with central velocity between −10 and +10 km s^{-1}.

https://doi.org/10.1071/AS00092 Published online by Cambridge University Press

Table 1. Southern Dark Cloud CO Catalogue

	RA(1950) [h m s]	Dec(1950) [° ′]	Density	Size [′]	T_A [°K]	V_{LSR} [km s^{-1}]	FWHM [km s^{-1}]	Desc. code
0.0–18.9	19 03 28	–37 18.4	A	16 x 5	10.5	5.4	2.0	c
0.3–18.8	19 03 22	–37 03.5	B	14 x 12	9.7	5.5	1.7	e/c
0.4–19.5	19 06 54	–37 12.4	A	16 x 7	6.2	5.7	1.8	e/c
0.8–22.9	19 23 45	–37 56.4	C	16 x 2	4.3	6.8	1.4	e/d-
0.9–20.2	19 11 02	–36 57.1	A	16 x 5	8.1	6.1	1.5	e
1.2–23.1	19 25 38	–37 40.7	C	5 x 4	2.1	6.9	1.7	d+
1.3–20.5	19 13 04	–36 41.7	A	14 x 4	8.2	5.9	1.2	a
1.4–21.6	19 18 23	–37 00.8	C	40 x 35	8.8	5.7	1.8	e/c
1.5–24.0	19 30 05	–37 37.4	C	4 x 3	-	-	-	
1.7–23.8	19 29 35	–37 25.2	C	3 x 3	4.3	9.6	1.0	a
4.9–24.6	19 37 23	–34 54.6	A	16 x 3	5.8	–1.5	0.8	a
8.4–47.1	21 29 21	–36 04.7	B	6 x 2	-	-	-	
9.0–46.5	21 26 23	–35 37.7	C	8 x 5	-	-	-	
10.4–46.6	21 27 17	–34 40.7	B	12 x 2	-	-	-	
10.5–47.1	21 29 41	–34 39.2	B	3 x 2	-	-	-	
247.0 –5.7	07 35 08	–32 37.3	B	22 x 2	4.3	20.6	2.5	dd
247.5–12.3	07 07 54	–36 07.4	B	65 x 55	11.1	2.4	1.6	e
247.6 –3.5	07 45 33	–32 05.5	B	7 x 5	6.4	18.7	1.2	a
247.8 –3.2	07 47 15	–32 04.8	B	6 x 1	5.6	18.7	2.0	dd
249.0 –3.2	07 49 59	–33 08.0	B	16 x 12	7.2	17.2	2.5	e
					2.5	26.2	1.0	c
249.4 –5.1	07 43 18	–34 28.9	A	4 x 2	18.1	7.2	1.5	e
					1.9	18.2	2.0	b
249.7 –2.1	07 56 09	–33 10.1	A	6 x 6	5.7	15.6	1.5	e
250.8 –8.1	07 33 35	–37 08.7	B	9 x 2	1.5	–1.0	1.6	dd
251.1 –1.0	08 04 16	–33 45.2	A	12 x 6	6.5	9.6	2.2	b
251.5 +2.0	08 17 26	–32 28.5	C	3 x 2	5.7	25.1	2.1	b
251.7 +0.2	08 10 29	–33 36.6	A	4 x 2	9.1	5.1	0.6	a
251.7–12.2	07 17 06	–39 45.6	B	4 x 3	11.3	–1.3	2.1	e
251.8 +0.0	08 10 25	–33 47.2	A	3 x 1	2.4	5.6	0.8	a
251.9 +0.0	08 10 27	–33 52.0	A	5 x1.2	6.8	5.4	0.8	a
252.1 –3.6	07 56 17	–35 56.5	B	12 x 7	2.1	–2.0	1.2	b
					17.1	7.2	2.3	dd
					1.5	14.5	4.2	b
252.1 –1.3	08 05 56	–34 46.0	B	22 x 12	8.6	12.9	3.0	dd
252.2 +0.7	08 14 03	–33 41.5	A	7 x1.2	6.9	1.6	0.6	a
252.3 +0.5	08 13 32	–33 55.5	A	6 x0.6	-	-	-	
252.3 –3.2	07 58 36	–35 55.5	A	14 x 9	18.4	8.5	2.0	dd
					3.5	12.5	0.8	a
252.5 +0.1	08 12 26	–34 21.7	A	10 x1.5	6.1	4.4	0.8	a

see http://www.atnf.csiro.au/pasa/17_1/otrupcek/table1.html

https://doi.org/10.1071/AS00092 Published online by Cambridge University Press

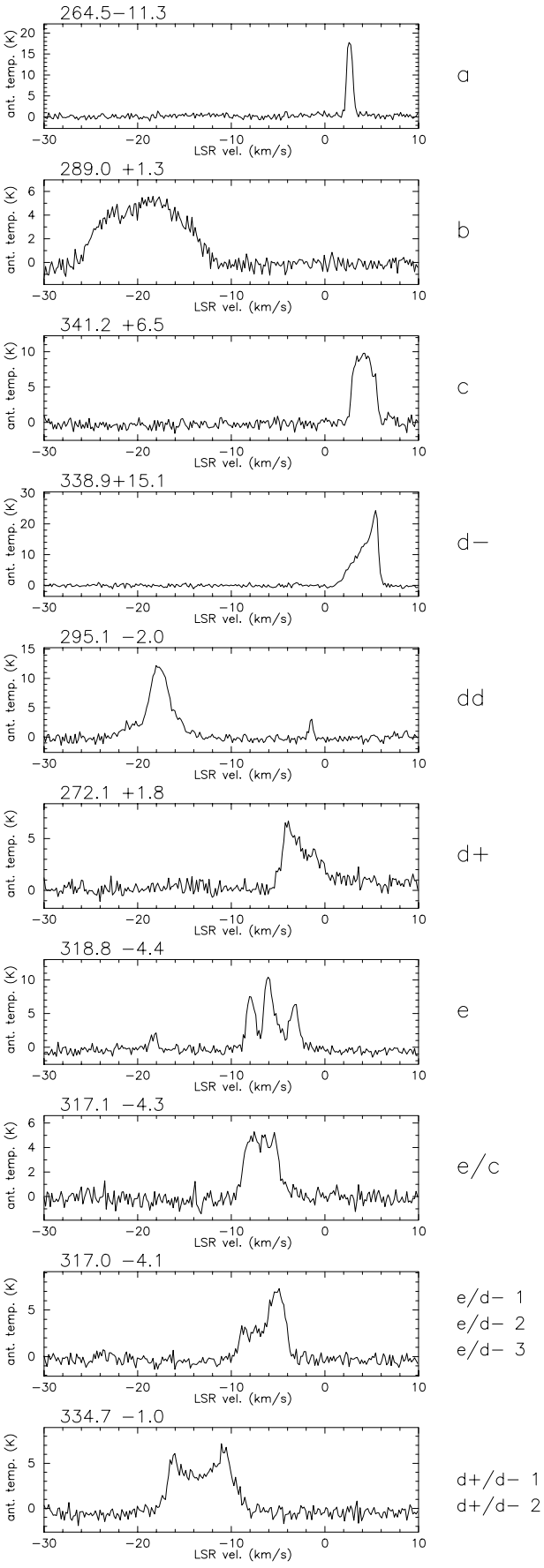

Figure 1—Example line profiles for each code. A full description is given in the text.

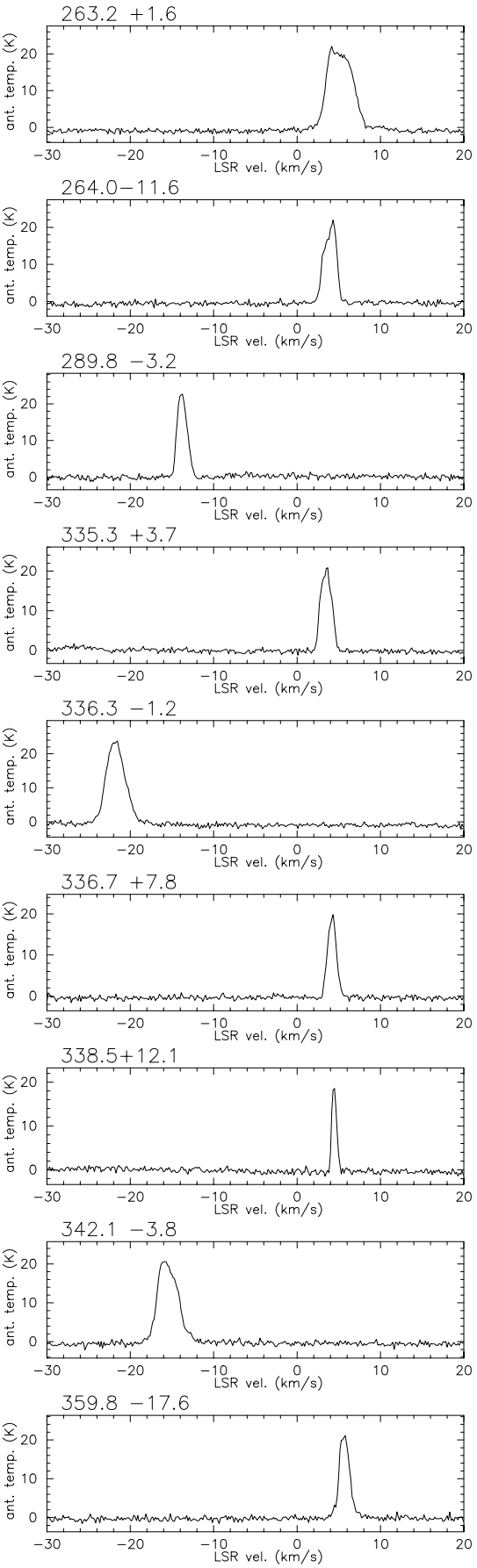

Figure 2—CO clouds with T_A^* greater than 20·0 K.

https://doi.org/10.1071/AS00092 Published online by Cambridge University Press

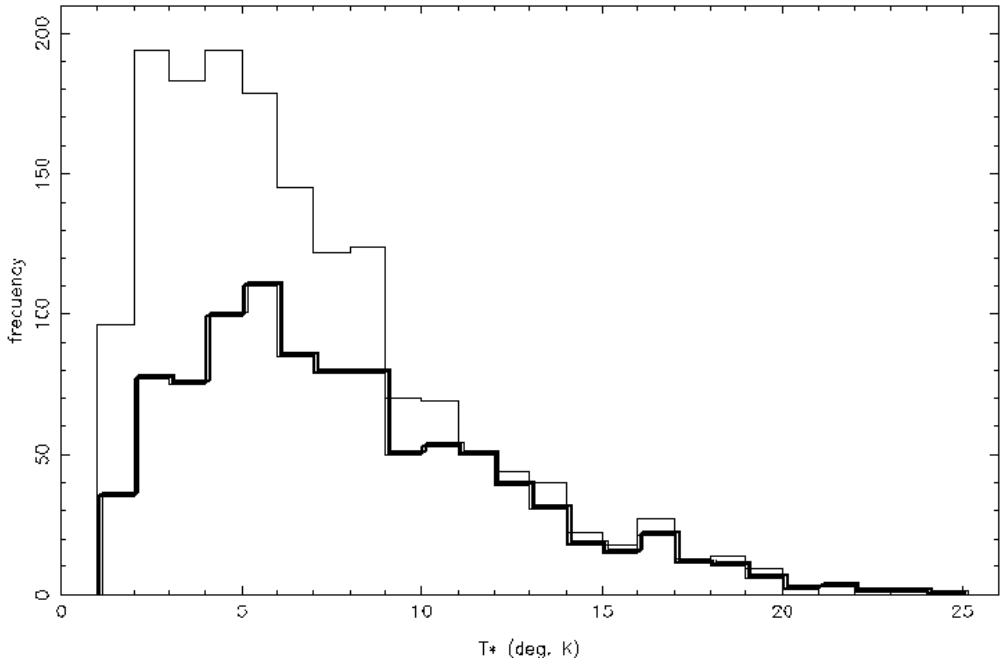

Figure 3—Distribution of T_A^*. The thin line is the distribution of all 1623 features, the thick line the distribution of 946 features with velocity -20 to $+10$ km s^{-1}, and width < 3 km s^{-1}.

They suggest a cold cloud in a quiescent state, and the emission in these profiles is most likely associated with the optical dark clouds.

b: broad, rounded, non-Gaussian spectra with FWHM—usually $>2{\cdot}0$ km s^{-1}. These profiles occurred across the velocity range but were usually at velocities more negative than $-10{\cdot}0$ km s^{-1}. They were often found in the direction of HII regions, or along the line of sight of a spiral arm in the Galactic Plane (see Robinson et al. 1988).

c: straight-sided profiles with a square top, broader than class 'a', with an FWHM usually between $1{\cdot}0$ and $2{\cdot}0$ km s^{-1}, an rms of Gaussian fit $>0{\cdot}5$ km s^{-1} and a central velocity usually between $-10{\cdot}0$ and $+10{\cdot}0$ km s^{-1}. They suggest an optically thick dark cloud (see Morris 1975), or a cloud with turbulence or expansion. The occurrence of these profile shapes should correlate highly with grade 'A' density clouds in the SDC catalogue.

d: Gaussian-shaped spectra, but with additional wings. Detections usually lie in the velocity range of $-20{\cdot}0$ to $+20{\cdot}0$ km s^{-1}. The profile shapes could be caused by a blending of narrower Gaussian features in the same line of sight with slightly shifted velocities (as described in code 'e'). Where possible we have fitted more than one Gaussian to the emission. Alternatively, they might indicate outflows or bipolar characteristics (Lada 1985), as are often found in star-forming regions. The numbered subdivisions denote the direction of the wings.

d−: blue-shifted wing (in the direction of decreasing velocity).

dd: wings on both sides of main component.

d+: red-shifted wing (in the direction of increasing velocity).

e: blended Gaussian shape of several narrow components. If one component has lower amplitude and is almost merged with another, the result can look like a 'd' shaped spectrum. If there are several components of similar intensity, they can look like a 'c' or even a 'b' shaped spectrum.

e1: a complex emission shape that requires more than one Gaussian.

e2: the components have separate fitted Gaussians that are numbered. The description code applies to the combined emission.

Figure 1 shows seven characteristic profile shapes, and three profiles, the description of which fits more than one category. In the case of the last three, the profile was coded with all possible categories; the most suitable one is listed first.

4 Discussion

4·1 CO Properties of the SDC

The nine strongest CO clouds ($>20{\cdot}0$ K) occurred at positions spread across the range of l^{II} and b^{II}.

https://doi.org/10.1071/AS00092 Published online by Cambridge University Press

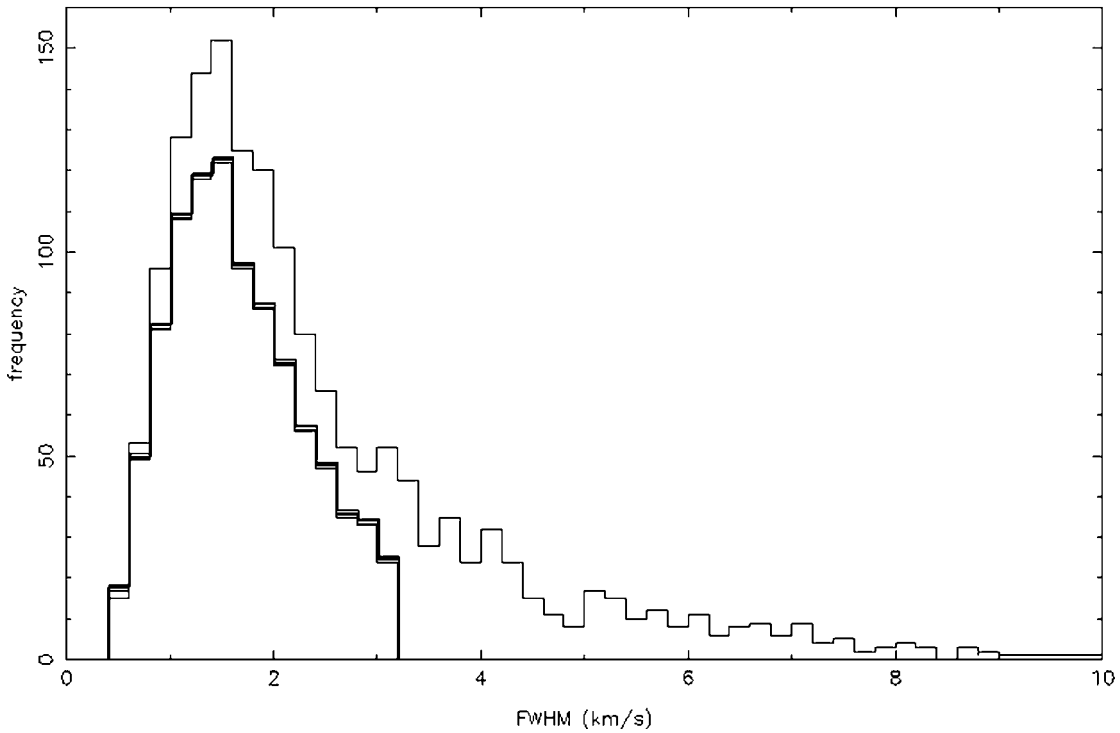

Figure 4—Distribution of linewidths (FWHM). The thin line is for all 1623 observations, the thick line those observations with velocity −20 to +10 km s^{-1} and width <3 km s^{-1}. (There are 30 observations with widths between 10 and 22 km s^{-1}.)

Their profile shapes are 'a' or 'd', and the dark clouds in these directions were listed in the Hartley et al. catalogue as Class A, the most visually opaque clouds. Their LSR velocities are near zero and the emission has very little structure to it (see Figure 2).

The 3σ level of the determination of T_A^* in our observations was 1·5 K and we chose this value as our detection cut-off; T_A^* ranged from this value to 25 K with 62% of these detections lying between 1·5 and 7·0 K.

Figure 3 contains a histogram of the temperature distribution; the lower heavier line is the temperature distribution of those observations lying in the velocity range of −20 and +10 km s^{-1} and having a linewidth less than 3·0 km s^{-1}. The curves are similar for sources with emission greater than 10 K suggesting that low velocity clouds are nearer and have stronger emission.

The median linewidth was 1·9 km s^{-1}, 66% lying between 1·0 and 3·0 km s^{-1} for all velocities, the narrowest being 0·4 km s^{-1} (see Figure 4). The heavier line shows the distribution of the observations with velocities lying in the range −20 to +10 km s^{-1}. The histogram for the sources with velocities between −20 and 10 km s^{-1} has a similar shape to the overall histogram for FWHM values less than 3·0 km s^{-1}. These narrow linewidths are to be expected as dark cloud positions were targeted.

A total of 72% of our detections have velocities between −20·0 and +10·0 km s^{-1}, the stronger signals lying between 5·0 and 10·0 km s^{-1} (see the distribution of velocities compared with the intensities in Table 2). The same divisions of velocity have been separated into divisions of linewidth in Table 3. These results show that narrow linewidths occur more frequently at velocities closer to zero km s^{-1}, which would be expected for a predominantly local dark cloud CO population. The detections with broader linewidths are at larger negative velocities, and the lines of sight here include the CO from giant molecular clouds (GMC) in different spiral arms (Blitz 1991).

The results are those expected if the sample contains a large proportion of nearby dark cloud CO (as distinct from CO emission from GMC). The distributions displayed in Table 3 can be further separated into subdivisions of profile-shape code (as described above and displayed in Figure 1, except that, in this table, the blended Gaussian shapes are denoted by the letter 'n'). Table 4 does this separation, but it should be noted that only the first code assigned to any particular profile was used.

Table 4 shows that the sample contains two well-defined subsets. One population lies in the velocity range −20 to +10 km s^{-1}, the profiles have a linewidth less than 3·0 km s^{-1}, they are likely to be 'a' type profiles if very narrow, or 'c' or 'd' type if less narrow, and have a higher T_A^*. The second population lies in the velocity range −95 to −10 km s^{-1}, the profiles have a linewidth greater than 3·0 km s^{-1}, and they are likely to be 'b' type profiles and have a lower T_A^*.

https://doi.org/10.1071/AS00092 Published online by Cambridge University Press

Table 2. Distribution of velocity (across) and intensities (down)

	-95 to -50 km s^{-1}	-50 to -30 km s^{-1}	-30 to -20 km s^{-1}	-20 to -10 km s^{-1}	-10 to -5 km s^{-1}	-5 to 0 km s^{-1}	0 to 5 km s^{-1}	5 to 10 km s^{-1}	10 to 43 km s^{-1}	TOTAL
0-5° K	58	107	71	89	86	90	72	52	42	667
5-10° K	20	34	59	91	68	115	95	128	30	640
10-25° K	1	8	17	15	12	42	85	128	8	316
TOTAL	79	149	147	195	166	247	252	308	80	1623

Table 3. Distribution of *V*(LSR) (across) and FWHM (down)

	-95 to -50 km s^{-1}	-50 to -30 km s^{-1}	-30 to -20 km s^{-1}	-20 to -10 km s^{-1}	-10 to -5 km s^{-1}	-5 to 0 km s^{-1}	0 to 5 km s^{-1}	5 to 10 km s^{-1}	10 to 43 km s^{-1}	TOTAL
0-1° K	0	2	4	8	16	40	44	45	5	164
1-2° K	6	21	46	83	74	117	126	160	36	669
2-3° K	11	23	35	42	47	46	53	66	22	345
3-5° K	19	46	39	47	21	31	25	34	11	273
5° K	43	57	23	15	8	13	4	3	6	172
TOTAL	79	149	147	195	166	247	252	308	80	1623

Table 4. Distribution of *V*(LSR) against FWHM separated by spectral shape code

	code	-95 to -50 km s^{-1}	-50 to -30 km s^{-1}	-30 to -20 km s^{-1}	-20 to -10 km s^{-1}	-10 to -5 km s^{-1}	-5 to 0 km s^{-1}	0 to 5 km s^{-1}	5 to 10 km s^{-1}	10 to 43 km s^{-1}	TOTAL
	a	0	0	2	6	11	35	33	31	4	122
	b	0	0	0	0	0	0	0	0	0	0
0-1° K	c	0	0	0	0	0	0	0	0	0	0
	d	0	1	0	1	1	2	1	2	0	8
	e	0	0	0	1	0	0	2	1	0	4
	n	0	1	2	0	4	3	8	11	1	30
	a	0	2	7	5	7	26	25	41	4	117
	b	2	1	1	0	0	2	1	1	2	10
1-2° K	c	0	0	0	6	3	5	8	20	3	45
	d	2	12	30	42	33	43	53	50	20	285
	e	0	3	2	15	7	21	9	20	5	82
	n	2	3	6	15	24	20	30	28	2	130
	a	0	0	0	0	0	0	0	0	0	0
	b	4	6	0	0	3	2	0	1	3	19
2-3° K	c	0	1	1	13	3	6	5	9	1	39
	d	5	12	17	16	21	27	28	31	11	168
	e	1	2	11	8	14	9	10	8	4	67
	n	1	2	6	5	6	2	10	17	3	52
	a	0	0	0	0	0	0	0	0	0	0
	b	11	12	6	2	5	1	3	1	6	47
3-5° K	c	0	2	1	2	0	3	2	2	0	12
	d	5	15	8	15	5	10	1	11	2	72
	e	1	6	12	19	8	13	8	5	3	75
	n	2	11	12	9	3	4	11	15	0	67
	a	0	0	0	0	0	0	0	0	0	0
	b	0	32	7	7	4	8	3	1	5	97
5° K	c	0	0	0	0	0	0	0	0	0	0
	d	7	4	2	0	1	4	0	1	0	19
	e	1	10	5	5	1	1	0	1	1	25
	n	5	11	9	3	2	0	1	0	0	31

https://doi.org/10.1071/AS00092 Published online by Cambridge University Press

Table 5. Distribution of FWHM and intensities of 946 features within the velocity range –20 to +10 km s^{-1}

	0.4 to 1 km s^{-1}	1.1 to 1.5 km s^{-1}	1.6 to 2.0 km s^{-1}	2.1 to 2.5 km s^{-1}	2.6 to 3.0 km s^{-1}	TOTAL
1.5 - 2.5° K	17	23	17	11	12	80
2.6 - 5.0° K	31	70	59	36	28	224
5.1 - 7.5° K	44	60	58	37	24	223
7.6 - 10° K	40	56	41	21	13	171
10.1 - 15° K	48	63	40	21	10	182
15.1 - 25° K	16	28	15	2	5	66
TOTAL	196	300	230	128	92	946

These are not mutually exclusive populations: 68% of the 1101 SDC catalogue positions have CO detections between −20 and +10 km s^{-1}, and linewidths less than 3·0 km s^{-1}. In view of these low velocities, these detections are most likely to be intrinsically associated with the nearby visual dark clouds along each line of sight, the detectability of which is limited by the interstellar medium. These clouds are relatively close to the Sun, and therefore produce CO emission at an LSR velocity closer to zero than more distant sources do. The adopted range has a bias towards the negative velocity because the rotation of the Galaxy in this quadrant of the Galactic Plane (247°–365°) results in negative velocities for clouds with galacto-centric radii shorter than the Sun.

The estimated distance from the Sun is ambiguous for the clouds with low velocities, as sources of a given velocity and Galactic longitude could be situated on either the near or the far side of the Galactic Centre, and a small fraction of the CO detections in the direction of the dark cloud positions may be at a greater distance.

A total of 55 entries in the velocity range −20 to 10 km s^{-1} have linewidths greater than 5·0 km s^{-1} and, of these, 30 have the 'b' shaped profile, and 41 have another CO component at a velocity outside this range. It would be safe to assume the CO was emitted from a GMC and exclude these 55 entries when attempting to find a subset of observations associated with the nearby visual dark clouds.

The second population of the original 1623 features are additional detections along the line of sight of the dark cloud positions, and likely to be more distant CO emission from giant molecular clouds, HII regions, or other CO clouds along the spiral arms. These entries are not a complete population of such molecular clouds, as there are many more CO clouds that are not coincident with the dark cloud directions.

4·2 Dark Cloud Observations

Within the velocity range −20 to +10 km s^{-1}, and linewidth limit of 3·0 km s^{-1}, there are 993 detections of independent features; 229 of these are additional clouds at the same position, and 47 are at positions marking the centre of complex collections of smaller dark clouds, and are unlikely to describe the nature of these smaller dark clouds. The distributions of T_A^* and linewidth of the relevant subset of 946 features, compared with the 1623 features in the full set can be seen in Figures 3 and 4. The quartile range of temperatures in this subset is 4·4 to 10·2 K (with a median of 6·8 K), and of linewidths it is 1·1 to 2·0 km s^{-1} (with a median of 1·5 km s^{-1}). The subset described above and listed in Table 5 gives the characteristics of the true dark cloud CO emission.

Dark cloud complexes. In the Hartley et al. catalogue, there are 48 positions considered to be the centre of complex regions that contain several smaller concentrations, such as those described by Kramer et al. (1993) and Williams, de Geus & Blitz (1993). These centres were denoted by a 'C' after the Galactic coordinate name given in the Hartley et al. catalogue, and the associated concentrations were noted in the comment column. These extended groups enabled us to examine the differences in shapes of the profiles of the smaller clouds associated with a larger complex region. We selected two examples of complex regions to demonstrate these differences.

As one moves spatially across the complex cloud, the profile shape changes from two peaks to one, as Figures 5 and 6 show. This could be emission from separate clouds in the same line of sight separated by distance, with maximum intensities occurring at different positions, or it might represent systematic changes in a single cloud. The clouds observed in Figure 5 are in the same line of sight

https://doi.org/10.1071/AS00092 Published online by Cambridge University Press

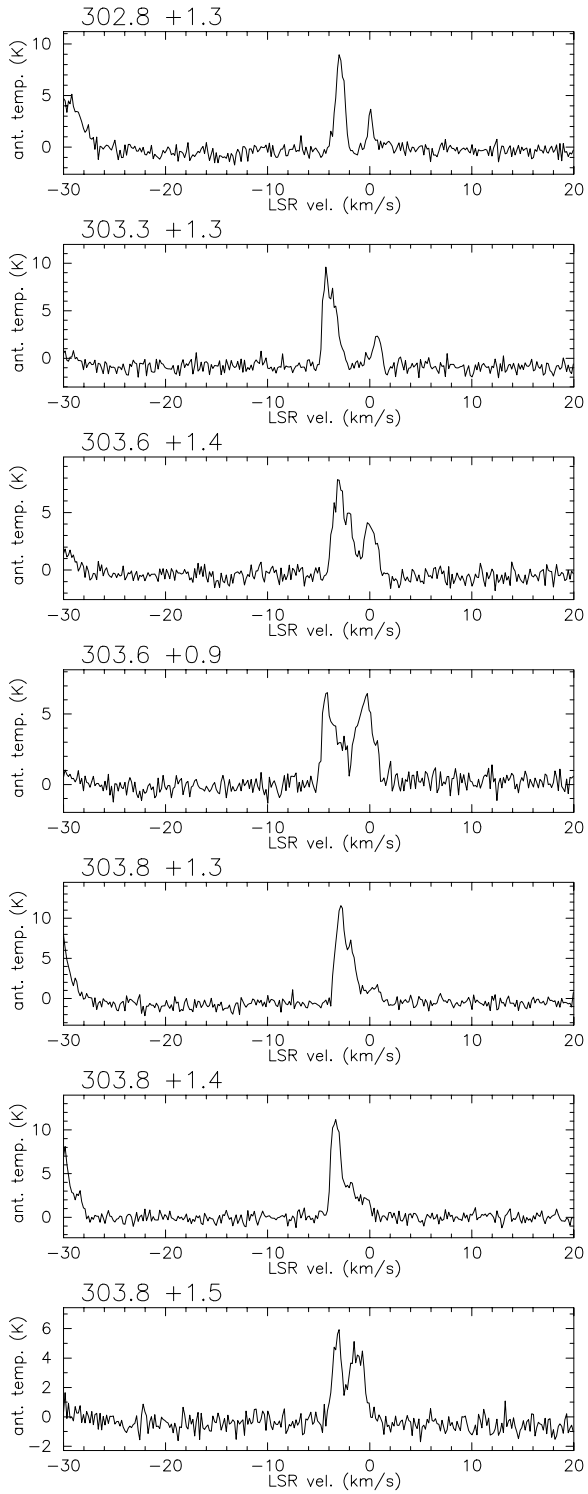

Figure 5—Small clouds associated with the DC303·8 +1·3C complex region.

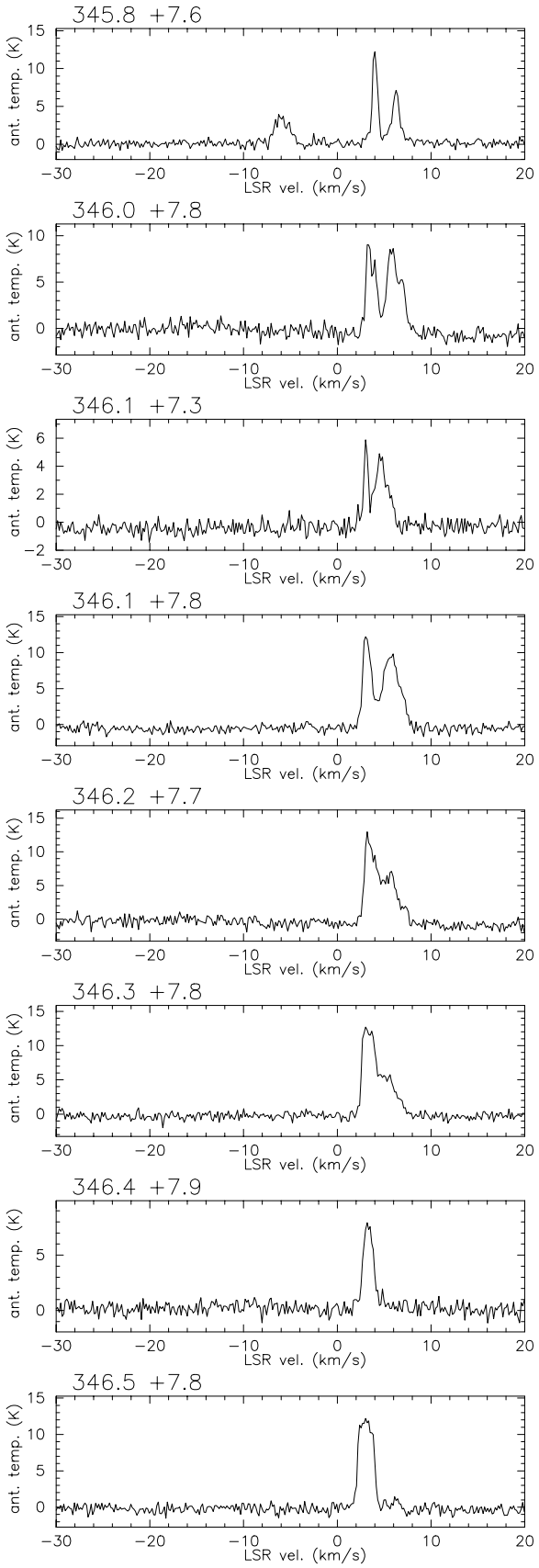

Figure 6—Small clouds associated with the DC346·2 +7·7C complex region.

https://doi.org/10.1071/AS00092 Published online by Cambridge University Press

as the Coalsack, which is a very fragmented cloud consisting of clumps and filaments and for which, as yet, there is no evidence of star formation (Nyman 1991). Fully sampled mapping of the complex cloud groups is required to determine their nature and stage of development.

5 Conclusions

The results have provided several conclusions which are listed below.

(1) Most dark cloud directions have CO. Emission was detected at 1049 of the 1101 dark cloud positions. At those 1049 positions there were 1623 separate CO emission features. 75% of non-detections were associated with least visually opaque (class C) clouds in the SDC.

(2) The features of the detections fit into well-defined groups. The shape of the CO spectral profiles enabled us to differentiate between narrow, broad rounded, square-topped, red- or blue-shifted wings, or both, and overlapping signals.

(3) There is a correlation between intensity, velocity and linewidth. The strongest signals are more likely to occur at low velocities (-20 $<+10$ km s^{-1}) and have narrower linewidths (<3 km s^{-1}). The weaker signals are more likely to occur at high negative velocities (<-20 km s^{-1}) and have broader linewidths (>3 km s^{-1}), which could be due to emission from more distant sources (e.g. GMCs) in the same line of sight as the targetted dark clouds.

(4) The distributions of velocity (LSR) against linewidth (FWHM) show two well-defined subsets. 68% of the positions have detections within the velocity range -20 to $+10$ km s^{-1}, and linewidths <3 km s^{-1}. It is evident that these detections are associated with the dark cloud positions, the definitions of which are limited by the optical detectabilty, and are likely to be within the 2-kpc range (Bok 1977). The population with broader linewidths and larger negative velocities are additional detections along the same line of sight as the visible dark clouds, but lying at greater distances. These detections most likely arise from GMCs within the spiral arms.

(5) The dark cloud detections have a $T_{\rm A}^{*}$ quartile range of $4{\cdot}4$ to $10{\cdot}2$ K (median of $6{\cdot}8$ K), and a linewidth quartile range of $1{\cdot}1$ to $2{\cdot}0$ km s^{-1} (median of $1{\cdot}5$ km s^{-1}). This subset contains 92% of the 'a' shape features (of the full range) and 81% of the 'c' shape features.

(6) Complex regions show changes of profile shape across them. Double-peaked profiles changed into single-peaked profiles with changing Galactic longitude for several of the complex regions, where smaller concentrations within larger clouds were given separate entries in the Hartley et al. catalogue. This may be caused by emission from separate clouds in the same line of sight separated by distance and whose maximum $T_{\rm A}^{*}$ occurs at different positions. On the other hand, it might represent systematic changes in a single cloud.

This catalogue may prove to be a starting point for a search for star-forming regions if candidates for mapping observations are selected from those positions demonstrating potential gas flows or systematic changes across adjacent components of complex regions.

Acknowledgments

The authors thank the Australian–Chinese collaborative agreement for its support of Professor Wang's visit, Dionne James from the UK Schmidt telescope (Siding Spring Observatory) for assisting with the observations, and Dr John Whiteoak (ATNF), Professor Jan Palous (Charles University, Prague) and Dr Tom Wilson (Max Planck Institut fur Radioastronomie, Bonn) for valuable discussions.

References

Blitz, L. 1991, in The Physics of Star Formation and Early Stellar Evolution, ed. C. J. Lada & N. D. Kylafis (Dordrecht: Kluwer), p. 3

Bok, B. 1977, PASP, 89, 597

Goss, W. M., Manchester, R. N., Brooks, J. W., Sinclair, M. W., & Manefield G.-A. 1980, MNRAS, 191, 533.

Hartley, M., Manchester, R. N., Smith, R. M., Tritton, S. B., & Goss, W. M. 1986, A&AS, 63, 27

Kramer, C., Zimmermann, T., Stutzki, J., & Winnewisser, G. 1993, in The Physics and Chemistry of Interstellar Molecular Clouds, ed. G. Winnewisser & G. Pelz (Berlin: Springer), p. 132

Lada, C. J. 1985, ARA&A, 23, 267

Morris, M. 1975, AJ, 197, 603

Nyman, L. A. 1991, in Low Mass Star Formation in Southern Molecular Clouds, ESO Scientific Report 11, ed. B. Reipurth, p. 119

Robinson, B. J., Manchester, R. N., Whiteoak, J. B., Otrupcek, R. E., & McCutcheon, W. H. 1988, A&AS, 193, 60

van Dishoeck, E. F., & Black, J. H. 1987, in Physical Processes in Interstellar Clouds, ed. G. E. Morfill & M. Scholer (Dordreicht: Reidel), p. 241

Williams, J., de Geus, E., & Blitz, L. 1993, in The Physics and Chemistry of Interstellar Molecular Clouds, ed. G. Winnewisser & G. Pelz (Berlin: Springer), p. 312

Wilson, W. E., Davis, E. R., Loone, D. G., & Brown, D. R. 1992, J. Electr. Electron. Eng. Aust., 12, 187

https://doi.org/10.1071/AS00092 Published online by Cambridge University Press